Journal of Materials Chemistry B

ROYAL SOCIETY OF CHEMISTRY

PAPER

View Article Online
View Journal | View Issue

Cite this: J. Mater. Chem. B, 2020, 8, 11010

A multi-model, large range and anti-freezing sensor based on a multi-crosslinked poly(vinyl alcohol) hydrogel for human-motion monitoring†

Yafei Gao,[a] Junbo Peng,[a] Manhua Zhou,[a] Yanyu Yang,*[a] Xing Wang,[b] Jianfeng Wang,[a] Yanxia Cao,[a] Wanjie Wang*[a] and Decheng Wu*[c]

Conductive hydrogels are capturing intensive attention for versatile applications in flexible wearable devices on account of their unique combination of softness, stretchability, conductivity and biocompatibility. However, most of the hydrogel sensors can only serve as single-type sensors to detect strain or pressure, accompanied by a limited detection range. Moreover, the poor anti-freezing performance is also a serious problem to be addressed for their practical applications. Herein, a multi-model, large range and anti-freezing hydrogel sensor was constructed from a high-mechanical and ionic conductive multi-crosslinked poly(vinyl alcohol) (M-PVA) hydrogel, which was prepared *via* incorporating chain entanglement interaction and complexation between Fe^{3+} ions and hydroxyl groups into the microcrystalline network through immersion treatment in $Fe_2(SO_4)_3$ solution. The three reversible and reconstructable crosslinks within the M-PVA hydrogel worked in tandem to achieve ultra-stretchability (1120%), supercompressibility (98%), high toughness, fast self-recoverability and excellent fatigue resistance. Meanwhile, the introduction of Fe^{3+} and SO_4^{2-} ions endowed the M-PVA hydrogel with good ionic conductivity and remarkable anti-freezing properties (−50 °C), which benefited the M-PVA hydrogel to act as a freezing-tolerant dressing. The assembled multi-model hydrogel sensor can sensitively and stably detect large range elongation (~900%), compression (~70%), bend and pressure (up to 4.60 MPa) concurrently, as well as various human activities including speaking, finger bending and treading behavior. Notably, the hydrogel sensor was capable of maintaining excellent mechanical flexibility and sensitive sensing capacity at low temperature. The M-PVA hydrogel is a promising flexible sensing material for versatile applications in ionic skin, motion recognition and intelligent wearable devices.

Received 17th September 2020,
Accepted 26th October 2020

DOI: 10.1039/d0tb02250k

rsc.li/materials-b

1. Introduction

Flexible sensors have drawn enormous attention in recent years due to their promising potential in human–machine interfacing,[1,2] health monitoring,[3–5] smart robotics,[6–8] and epidermal and implantable electronics.[9,10] For example, wearable strain and pressure sensors can realize the monitoring of heartbeat, pulse and various motions by converting external stimuli into recordable electrical signals. Generally, flexible sensing materials are composed of elastic matrixes[11–13] (*e.g.*, polydimethylsiloxane and polyurethane) and conductive components[14–17] (*e.g.*, metal nanomaterials, carbon materials and conductive polymers). However, most of the current sensing materials possess high rigidity, producing a large discrepancy in stiffness with skins and other tissues.[18] Additionally, the sensing materials tend to be destroyed in response to large strain resulting from limited stretchability.[16,17] Hence, constructing soft and high-deformable sensing materials is of great significance for developing flexible wearable devices.

Conductive hydrogels possess a unique combination of excellent softness, stretchability, biocompatibility and electrical signal transduction capacity, being a type of predominant sensing material for flexible electronics.[18–24] The aqueous matrix of the hydrogel can render a conductive path to guarantee the convenient transmission of electrons or ions, and the elastic polymer network framework within the hydrogel is capable of sustaining various deformations. Recently, several conductive hydrogels have been developed to fabricate flexible sensors to detect various human motions.[25,26] In practice,

[a] College of Materials Science and Engineering, Zhengzhou University, Zhengzhou, Henan 450001, China. E-mail: yyyang@zzu.edu.cn, wwj@zzu.edu.cn
[b] Beijing National Laboratory for Molecular Sciences, Institute of Chemistry, Chinese Academy of Sciences, Beijing 100190, China
[c] Department of Biomedical Engineering, Southern University of Science and Technology, Shenzhen, Guangdong 518055, China. E-mail: wudc@sustech.edu.cn

† Electronic supplementary information (ESI) available. See DOI: 10.1039/d0tb02250k

flexible wearable sensors (*e.g.*, electronic skin) need to perceive strain (elongation, compression and bend), touched pressure and even a mix of both currently.[27] However, most of the hydrogel sensors can only serve as single-type sensors to detect either strain or pressure, which cannot meet the practical demands for detecting deformation and pressure together. In addition, a large detection range for both strain and pressure is required in hydrogel sensors for monitoring full-range human motions like walking and jumping. As a consequence, it is essential to develop multi-model and high-deformable hydrogel sensors for meeting the actual requirement and further broadening their applications.

Generally, conventional conductive hydrogels will inevitably enter a frozen state, and therefore lose mechanical advantages and conductivity at subzero temperature, which seriously impedes their applications in cold weather.[28] Currently, incorporating ionic compounds and binary solvent systems into hydrogels can effectively weaken the hydrogen bonding within water molecules and inhibit the formation of ice crystals, achieving anti-freezing hydrogels or organohydrogels.[29–32] Vlassak *et al.* introduced $CaCl_2$ solution into the dispersed medium of hydrogels and obtained low temperature tolerant polyacrylamide-alginate hydrogels with a freezing point of −57 °C.[29] When the temperature decreased to −30 °C, the fracture strain of the hydrogels still reached a high value of 350%. Lu *et al.* utilized glycerol/water binary solvent to fabricate poly(acrylamide-*co*-acrylic acid)/carbon nanotube organohydrogels, which still maintained outstanding stretchability at −20 °C.[33] Compared to binary solvents, incorporation of ions is an economical and eco-friendly strategy to fabricate freezing tolerant and conductive hydrogels without adding any conductive nanofillers.

Herein, a multi-model, high-deformable and anti-freezing hydrogel sensor was assembled from a multi-crosslinked poly(vinyl alcohol) (M-PVA) hydrogel with outstanding mechanical properties and good conductivity, which was prepared by incorporating chain entanglement interaction and complexation between Fe^{3+} ions and hydroxyl groups into the microcrystalline network through immersion treatment in $Fe_2(SO_4)_3$ solution (Fig. 1). The three reversible and reconstructable crosslinks within the M-PVA hydrogel worked in tandem to achieve ultra-stretchability (1120%), supercompressibility (98%), high toughness (48.5 MJ m^{-3}), fast self-recoverability and superior fatigue resistance. Meanwhile, the introduction of Fe^{3+} and SO_4^{2-} ions endowed the M-PVA hydrogel with good ionic conductivity and remarkable anti-freezing properties (−50 °C). The M-PVA hydrogel can be assembled as a multi-model sensor to detect large range elongation (~900%), compression (~70%), bend and touched pressure (up to 4.60 MPa). In addition, the hydrogel sensor can serve as a wearable sensor to detect full-range human activities, including speaking, finger bending and treading behaviors, even at low temperature. This work will pave the way for fabricating multi-model, freezing tolerant and large range hydrogel sensors for flexible electronics, intelligent devices and health monitoring.

2. Experimental section

2.1. Materials

Poly(vinyl alcohol) (PVA, M_n = 8.8 × 10^4 Da, 99% hydrolysis degree) was obtained from Shanxi Sanwei Co., Ltd. Ferric sulfate ($Fe_2(SO_4)_3$) was purchased from Sinopharm Chemical Reagent Co., Ltd. Deionized water was purified using a

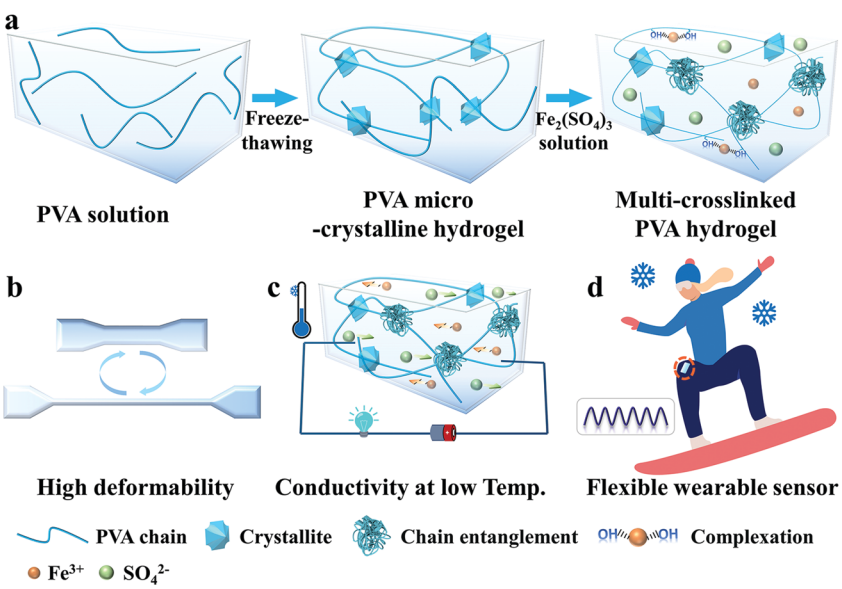

Fig. 1 Construction of high-deformable and anti-freezing multi-crosslinked poly(vinyl alcohol) (M-PVA) hydrogels and hydrogel-based multi-model wearable sensors. (a) Preparation process of the M-PVA hydrogels. (b) High-deformable M-PVA hydrogels to ensure large extension. (c) Good conductivity at subzero temperature *via* ionic migration. (d) Anti-freezing wearable hydrogel-based sensor to detect various human motions in cold weather.

Milli-Q purifier. All of the reagents were used without further purification.

2.2. Hydrogel preparation

Multi-crosslinked hydrogels were prepared *via* a facile and feasible two-step crosslinking strategy. Firstly, PVA powder (16.3 g) was dissolved in distilled water (100 mL) at 90 °C with vigorous stirring to form a transparent and homogeneous solution. After cooling to 60 °C, the PVA solution was injected into a glass mold and endured two freezing–thawing (F–T) cycles to obtain a PVA microcrystalline hydrogel (S-PVA, S refers to single microcrystalline crosslinking). The F–T cycles were implemented in the fridge at −20 °C for 12 h, followed by thawing at room temperature for 3 h. Subsequently, the S-PVA hydrogel was immersed in $Fe_2(SO_4)_3$ solution (0.4, 0.8, 1.2, 1.6 and 2.4 M) for 12 h to generate multi-crosslinked PVA hydrogels (M-PVA, M refers to multi-crosslinking).

2.3. Fabrication of the hydrogel-based flexible sensor

The hydrogel-based resistance-type sensor was assembled from one M-PVA hydrogel sample and two copper slices, wherein the M-PVA hydrogel served as an ionic conductor and the copper slices served as electrodes. A 3 M VHB tape was applied to encapsulate the hydrogel sensor to prevent water evaporation.

2.4. Characterization

The hydrogel samples were first frozen with liquid nitrogen and then freeze-dried for the following characterization. Focused ion beam scanning electron microscopy (FIB-SEM, Zeiss/Auriga-Bu*) was performed to analyze the microstructure of the hydrogels. X-ray diffraction (XRD) was performed using an X-ray diffractometer (DX-2700BH) equipped with a Ni-filtered Cu Kα radiation source (λ = 1.5405 Å) in the 2θ range of 5–60° with a scan rate of 5° min^{-1}. The crystallinity of the hydrogel samples was evaluated as the ratio between the area of crystalline reflection in the 2θ range 18–21° and the area subtending the whole diffraction profile.[22] Fourier transform infrared (FT-IR) nicolet iS50 spectroscopy (Thermo Fisher) was applied to record the FT-IR spectra. The static conductivity of the hydrogel samples was measured by the standard four-probe technique (RTS-8).

2.5. Mechanical test

The compressive and tensile properties of the hydrogels were measured using an Electronic Universal Testing Machine (UTM6104) with load cells of 10 kN and 500 N at a rate of 5 mm min^{-1} and 50 mm min^{-1}. The shapes of the hydrogel samples were rectangular (25 × 3.0 × 1.5 mm) and cylindrical (diameter: 10 mm, height: 12 mm), respectively. The rates of the loading–unloading test upon elongation and compression were 100 mm min^{-1} and 10 mm min^{-1}, respectively. The mechanical indexes (tensile strain, tensile stress, elastic modulus, toughness, *etc.*) were obtained according to the literature.[23]

The tensile properties of the hydrogels at low temperatures were measured at 50 mm min^{-1} using an Electronic Universal Testing Machine (UTM6104) with an environmental chamber (MTS GDX200), wherein the temperature was regulated by spraying liquid N_2 into the chamber. The specimens were held at the setting temperature for 30 min before the measurement.

2.6. Dynamic strain and pressure sensing measurements

The real-time resistance of the hydrogel sensors upon various deformations and pressures was obtained using a combined instrument consisting of an oscilloscope (Tektronix DMM4050 6-1/2 Digit Precision Multimeter) and an Electronic Universal Testing Machine (UTM6104). The rates of elongation and compression were 50 mm min^{-1} and 5 mm min^{-1}, respectively. The relative resistance change and the relative current change were defined as $\Delta R/R_0$ (%) = $(R - R_0)/R_0 \times 100$ and $\Delta I/I_0$ (%) = $(I - I_0)/I_0 \times 100$, respectively. The gauge factor was obtained from the slope of relative resistance change ($\Delta R/R_0$) *versus* strain, and the sensitivity was obtained from the slope of relative current change ($\Delta I/I_0$) *versus* pressure. In order to confirm the feasibility of being wearable sensors, the hydrogel sensors were attached to the face and joint of a volunteer to monitor various human motions.

2.7. *In vivo* experiment

Five male Sprague Dawley (SD) rats (310–320 g) were used for the frostbite test. The thickness of the hydrogel samples was fixed at 3 mm. The rats were anaesthetized *via* intraperitoneal injection of pentobarbital (2 wt%, 2 mL kg^{-1}). The hair was shaved and cleaned before testing. Three steel coins were immersed in liquid nitrogen for 30 min and then attached to the skins for 30 s. After the frostbite test, the rats were euthanized using excessive anesthesia and the back skins were removed and fixed in 10% formalin buffer for histological studies. The skin surface tissue was cut into vertical slices for cross-sectional observation. Finally, histological observations were made after hematoxylin-eosin (H&E) staining. All the above tests were conducted in accordance with the regulations approved by the local ethics committee and Chinese laboratory animal management regulations.

3. Results and discussion

3.1. Preparation of the M-PVA hydrogel

Fig. 1a illustrates the simple preparation process of the M-PVA hydrogel. Firstly, a transparent PVA solution (14 wt%) endured two freezing–thawing (F–T) cycles to fabricate a PVA microcrystalline hydrogel (S-PVA, S refers to single microcrystalline crosslinking). During the F–T cycles, the enhanced inter-chain hydrogen bonding promoted the generation of PVA crystallites, which acted as physical cross-linked sites of the microcrystalline network. Subsequently, the S-PVA hydrogel was immersed into $Fe_2(SO_4)_3$ solution to obtain an ionic conductive multi-crosslinked PVA-*X* hydrogel (M-PVA-*X*, M refers to multi-crosslinking, X refers to the concentration of $Fe_2(SO_4)_3$ solution). Upon treatment in $Fe_2(SO_4)_3$ solution, the salting out effect intensified the intermolecular interaction within the PVA chains, leading to inter-chain aggregation and chain-entanglement

joints within the hydrogel. Additionally, the osmotic pressure difference contributed to the volume shrinkage of the hydrogel, further enhancing the inter-chain aggregation within the hydrogels. Meanwhile, Fe^{3+} ions can combine with the hydroxyl groups of PVA chains to form dynamic complexing interaction.[34] As a consequence, a multi-crosslinked PVA network including microcrystalline crosslinking, chain-entanglement crosslinking and complexation was obtained. The chain entanglement and complexation between Fe^{3+} ions and hydroxyl groups can significantly improve the mechanical properties of the PVA hydrogel, resulting in supercompressibility and high stretchability (Fig. 1b). The Fe^{3+} and SO_4^{2-} ions permeating into the hydrogel can weaken the hydrogen bonding within the water molecules and hinder the formation of ice crystals, achieving mechanical flexibility and conductivity at low temperature (Fig. 1c). On account of the outstanding mechanical performance and remarkable freezing tolerance, the conductive M-PVA hydrogel can be utilized as a multi-model and anti-freezing wearable sensor to detect various human activities, even in a harsh environment (Fig. 1d).

3.2. Mechanical properties of the M-PVA hydrogel

The mechanical properties of conductive hydrogels, such as deformability, strength, toughness and durability, are important factors that make them flexible sensing materials.[35–37] As shown in Fig. 2a, the M-PVA hydrogel exhibited preeminent deformability to withstand different high-level deformations without fracture, such as compression, twisted stretching and knotting stretching. Notably, the M-PVA hydrogel can endure high pressure and quickly recover its initial shape after removal of the load, demonstrating superior elasticity and toughness. When the compressive strain was set at 98%, the M-PVA hydrogel still remained intact and the compressive stress achieved was 112.0 MPa, indicating impressive supercompressibiltiy. Meanwhile, the M-PVA hydrogel also exhibited high stretchability with a fracture strain of 1120%, and the tensile strength and toughness (curve area) achieved were high with values of 7.2 MPa and 48.5 MJ m^{-3}, respectively. Notably, a multiple crosslinked PVA hydrogel was first reported and its comprehensive mechanical performance exceeded that of most of the reported PVA hydrogels.[38,39]

In order to evaluate the effect of chain entanglement and complexing interaction on the improved mechanical performance of the PVA hydrogel, we fabricated single-, dual-, and multi-crosslinked PVA hydrogels and then measured their tensile properties (Fig. S1A (ESI†)), wherein a (b) dual-crosslinked PVA (D-PVA) hydrogel was prepared by immersing the PVA microcrystalline hydrogel into Na_2SO_4 solution and a (d) D-PVA hydrogel was prepared by altering the sequence of F–T cycles and immersion treatment in $Fe_2(SO_4)_3$ solution. As shown in Fig. S1A (ESI†), compared to (a) S-PVA, the (b) D-PVA hydrogel exhibited a striking enhancement in the mechanical performance, indicating that the enhanced chain entanglement was of vital significance for superior mechanics. Meanwhile, the comparison between (b) D-PVA and (c) M-PVA hydrogels shown in Fig. S1A (ESI†) confirmed the contribution of complexation to the improved mechanics. In addition, the (d) D-PVA hydrogel displayed slightly improved mechanical performance compared to the S-PVA hydrogel (Fig. S1B, ESI†), implying that the generated complexation impaired the formation of hydrogen bonding during the following F–T cycles.

The structures of the M-PVA hydrogels can be readily regulated by varying the concentration of $Fe_2(SO_4)_3$ solution. Upon treatment with $Fe_2(SO_4)_3$ solution, the crystallite was slightly dissociated and meanwhile the chain entanglement interaction was reinforced. The dissociation degree of crystallite and the reinforcement degree of chain entanglement were positively correlated with the concentration of $Fe_2(SO_4)_3$ solution (0.4, 0.8, 1.2, 1.6 and 2.4 M). The dissociation of crystallization can be explicitly revealed *via* the evolution of crystallinity and the hydrogen bonding interaction within the hydrogel using XRD and FTIR spectroscopy, respectively. As shown in Fig. S2a (ESI†), as the

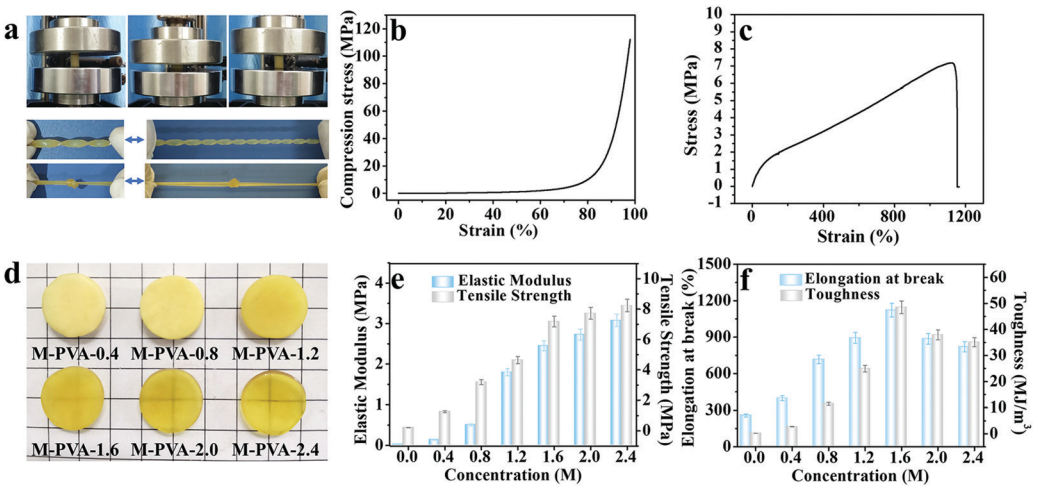

Fig. 2 (a) Photographs demonstrating the outstanding elasticity, compressibility and stretchability of the M-PVA-1.6 hydrogel. (b) Compressive and (c) tensile stress–strain curves of the M-PVA-1.6 hydrogel. (d) Photographs of the M-PVA hydrogels with different concentrations of $Fe_2(SO_4)_3$ solution. (e) Elastic modulus and tensile strength of the M-PVA hydrogels. (f) Fracture strain and toughness of the M-PVA hydrogels.

concentration of the $Fe_2(SO_4)_3$ solution increased, the crystallinity of the PVA hydrogels decreased gradually. The crystallinity of S-PVA, M-PVA-0.4, M-PVA-1.6 and M-PVA-2.4 was 34.9%, 23.8%, 20.4% and 18.1%, respectively. As for the FT-IR spectra shown in Fig. S2b (ESI†), the absorption band of the hydroxyl groups at 3384 cm^{-1} for the S-PVA hydrogel shifted towards a high wavenumber for the M-PVA hydrogels. The decreased crystallinity in the XRD profiles and the blue-shifting phenomenon in the FTIR spectra may be attributed to the slight weakening of hydrogen bonding within the PVA chains. Moreover, the SEM images of the S-PVA and M-PVA hydrogels display the evolution of the microstructure after treatment with $Fe_2(SO_4)_3$ solution. Compared with the S-PVA hydrogel, the M-PVA hydrogel possessed a denser microstructure with a higher cross-linking density and a smaller pore size (Fig. S3, ESI†). The striking contrast in the microstructure was ascribed to the post-formed chain entanglement and complexing interaction, together with slight volume shrinkage. Accompanied by the change of the interior structure, the M-PVA hydrogel became transparent gradually with the increasing concentration of $Fe_2(SO_4)_3$ solution (Fig. 2d).

The variation of the mechanical properties of the M-PVA hydrogels was consistent with the evolution of the structure. The enhanced chain entanglement and complexing interaction improved the rigidity and toughness of the M-PVA hydrogel. The elastic modulus and the tensile strength improved continuously with the increasing concentration of $Fe_2(SO_4)_3$ solution. When the concentration of $Fe_2(SO_4)_3$ was 2.4 M, the elastic modulus and the tensile strength reached high values of 3.1 MPa and 8.2 MPa, respectively, surpassing those of most of the previously reported hydrogels.[28,35,36] Notably, the elastic modulus of the M-PVA hydrogels (0.1–3.1 MPa, Fig. 2e) was able to match that of human tissue (10^4–10^9 Pa), benefiting their applications in artificial tissues.[17,40] The fracture strain increased quickly in the first stage resulting from the enhanced crosslinked interaction within the PVA hydrogels, and then decreased arising from the restricted movement of the PVA chains and the high cross-linked density (Fig. 2f). The toughness (curve area) displayed a similar change tendency. When the concentration of $Fe_2(SO_4)_3$ was 1.6 M, the fracture strain and toughness achieved maximum values of 1120% and 48.5 MJ m^{-3}, respectively. In this work, unless otherwise mentioned, the M-PVA-1.6 hydrogel (water content: 36.9 wt%, Table S1, ESI†) was used in the following investigation because of its optimized comprehensive properties (super-compressibility (98%), ultra-stretchability (1120%), high tensile strength (7.2 MPa) and high toughness (48.5 MJ m^{-3})).

Upon deformation, the multiple physical crosslinking within the M-PVA hydrogel can be dissociated to consume energy, improving the toughness of the M-PVA hydrogel.[41] A loading–unloading experiment was implemented to exactly evaluate the energy dissipation capacity of the M-PVA-1.6 hydrogel shown in Fig. 3a, and the area of the hysteresis loop represented the energy dissipated per unit volume. As the strain increased, the hysteresis loops became larger. The dissipated energy (U_{hys}) increased from 0.5 MJ m^{-3} at ε = 100% to 12.0 MJ m^{-3} at ε = 500% (Fig. 3b). Meanwhile, the dissipated energy coefficient increased to 88.4% at ε = 500%.

The reversible physical crosslinking can be repaired and reconstructed after damage, endowing the M-PVA hydrogel with excellent self-recovery ability. To investigate the self-recoverability, cyclic loading–unloading tests were performed on the stretched M-PVA-1.6 hydrogel after different resting times at a certain strain of 200%. Distinctly, compared with the original hydrogel sample, the stretched hydrogel sample demonstrated a much smaller

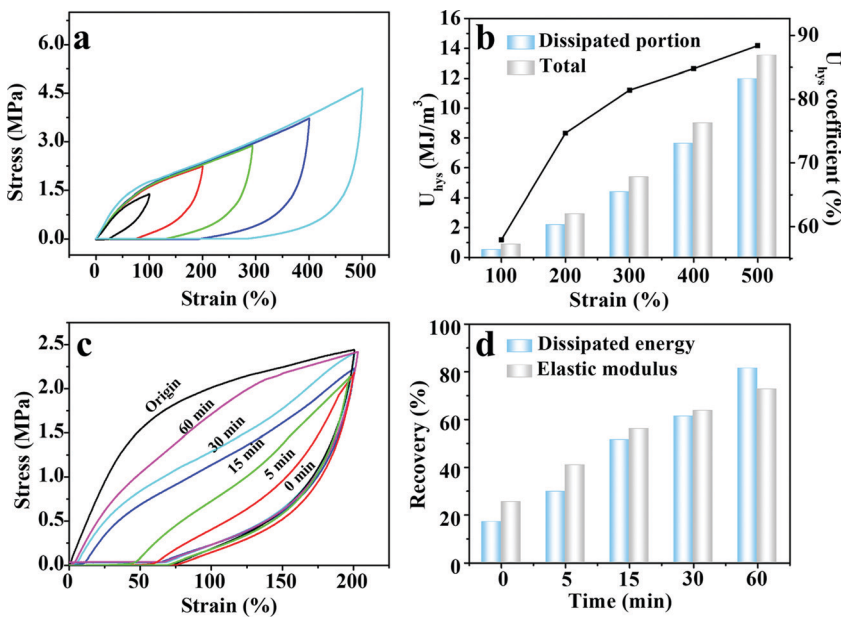

Fig. 3 (a) Loading–unloading curves of the M-PVA-1.6 hydrogel under different strains (100%, 200%, 300%, 400% and 500%). (b) Calculated dissipated energy and the energy dissipation coefficient of the M-PVA-1.6 hydrogel during the loading–unloading tests under different strains. (c) Stress–strain curves of the original and stretched M-PVA-1.6 hydrogel. (d) Time-dependent recovery of hysteresis and the elastic modulus.

hysteresis loop at the immediate second cycle, indicating that the destroyed physical crosslinking cannot be fully healed without resting (Fig. 3c). The immediate recovery efficiencies of energy hysteresis and the elastic modulus were 17.0% and 25.4%, respectively (Fig. 3d). With the increase of the resting time, the hysteresis loops gradually tended to the original one and the maximum stress also approached the original value. After relaxing for 60 min, the recovery efficiencies of energy hysteresis and the elastic modulus increased to 81.4% and 72.7%, respectively.

Remarkable softening resistance is of significance to the long-term application of hydrogel-based flexible devices.[42] As shown in Fig. 4a and d, 50 consecutive elongation–relaxation cycles (ε = 200%) and compression–relaxation cycles (ε = 50%) were implemented to investigate the repeated force-bearing ability of the M-PVA-1.6 hydrogel. The repeated curves in the 2nd–50th cycles as shown in Fig. 4a and d and the slightly decreased maximum load as shown in Fig. 4b and e strongly indicated the outstanding softening resistance, which was highly needed for the practical applications of hydrogels and hydrogel-based devices. The maximum stress and the dissipated energy (U_{hys}) every three cycles are summarized in Fig. 4c and f. The maximum tensile and compression stress after 50 continuous cycles still retained high values of 2.4 MPa (ε = 200%) and 0.9 MPa (ε = 50%), respectively. The dissipated energy of the 2nd–50th cycles remained stable in both elongation–relaxation cycles (0.2 MJ m^{-3}) and compression–relaxation cycles (18.0 kJ m^{-3}). These results suggested that the M-PVA hydrogel showed outstanding anti-softening performance and excellent mechanical stability, which will be conducive to the M-PVA hydrogel applied in repeated load-bearing areas, such as flexible electronics, actuators, soft robots and tissue engineering.

3.3. Flexible strain and pressure sensing performance

Upon treatment in $Fe_2(SO_4)_3$ solution, not only the generated chain entanglement and complexing interaction enhanced the mechanical performance of the PVA hydrogel, but also the incorporation of Fe^{3+} and SO_4^{2-} ions into the three-dimensional network provided ionic conductivity to the PVA hydrogel. As shown in Fig. S4 (ESI†), the M-PVA-1.6 hydrogel can be employed as an ionic conductor in a closed circuit to lit a light-emitting diode indicator. The conductivity of the M-PVA-1.6 hydrogel was 0.6 S m^{-1} at 25 °C. Due to the unique combination of stretchability, supercompressibility, softening resistance and ionic conductivity, the M-PVA hydrogel can be assembled into a multi-model and durable sensor to detect strain and pressure concurrently and repeatedly. As the hydrogel endured the deformation or pressure, the ionic channel changed and therefore affected the situation of ionic migration, resulting in varied conductivities. As a consequence, the M-PVA hydrogel sensor realized the transformation of mechanical deformation or force into recordable electrical signals. A combined instrument consisting of an oscilloscope and a universal tensile tester was applied to measure the dynamic resistance/current and investigate the sensing performance of the M-PVA hydrogel sensor. As shown in Fig. 5a, the resistance increased along with the tensile strain because of the extended ion migration distance and the narrow ionic channel during the stretching process. As the tensile strain was set at 5%, the response time of the hydrogel sensor during loading was about 0.43 s, while the response time during unloading was about 0.41 s (Fig. S5, ESI†). The gauge factor (GF) values of the M-PVA-1.6 hydrogel sensor were 2.4 and 3.8 in the strain range of 0–410% and 410–900%, respectively. Notably, the hydrogel sensor possessed a broad strain window (0–900%) with high sensitivity. Moreover, the hydrogel strain sensor exhibited good repeatable electrical signal responses on detecting both small strain and large strain (Fig. 5b and c). The slight baseline deviation under large strain (Fig. 5c) was ascribed to the residual strain under large strain. Significantly, the sensor exhibited excellent stability without obvious attenuation during 100 cyclic measurements at a strain of 100% (Fig. 5d).

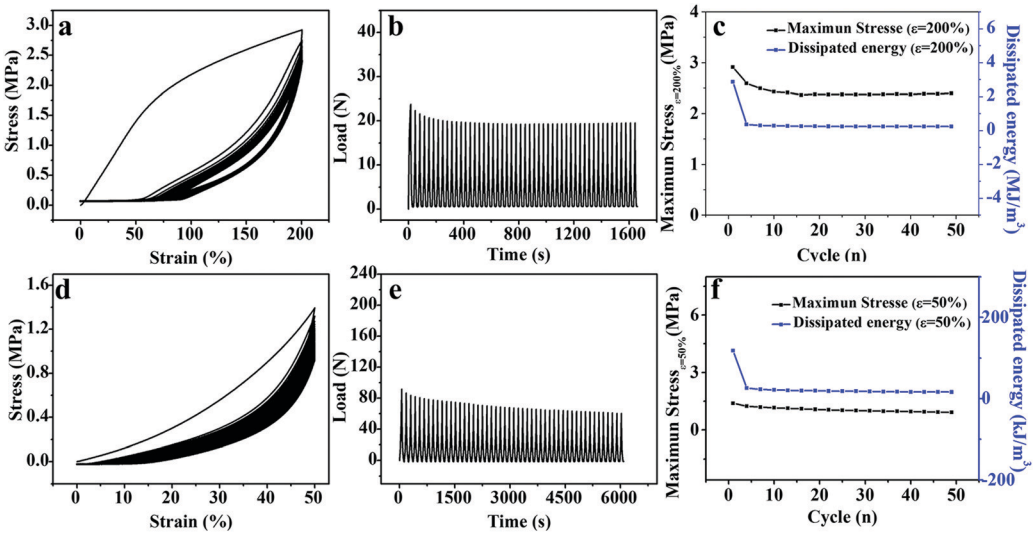

Fig. 4 (a and d) 50 successive stress–strain curves and (b and e) load–time curves of the M-PVA-1.6 hydrogel during (top) elongation–relaxation and (bottom) compression–relaxation cycles. (c and f) Evolution of maximal stress and dissipated energy during 50 continuous cycles.

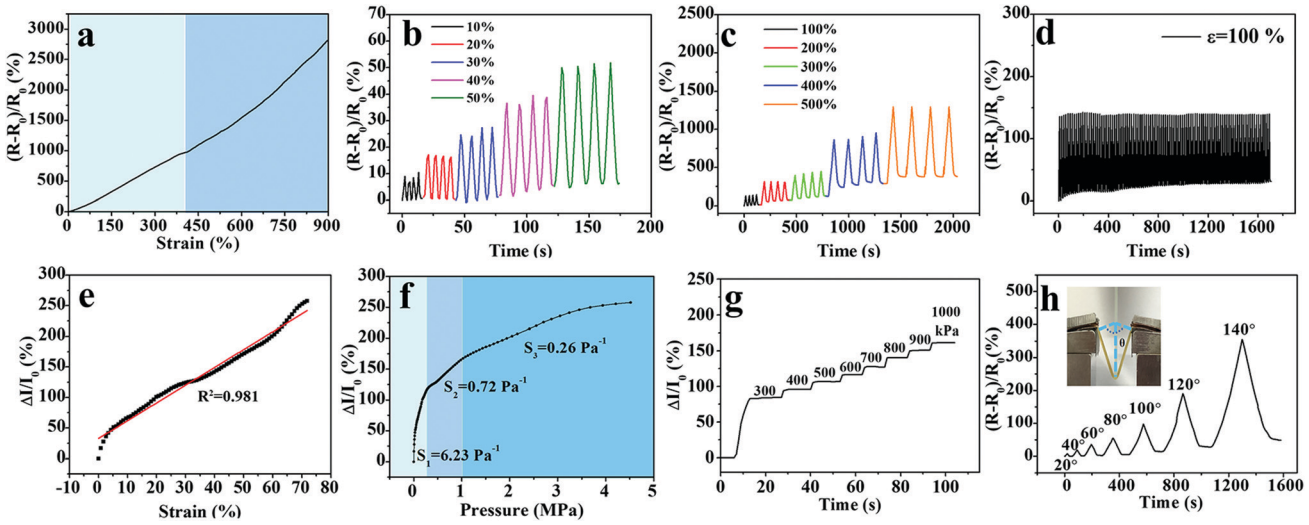

Fig. 5 Sensitive sensing performance of the multi-model M-PVA-1.6 hydrogel sensor. (a) Relative resistance changes of the hydrogel sensor during the stretching process. Time-dependent relative resistance changes upon (b) small strain and (c) large strain. (d) 100 cycling tests at a maximum strain of 100%. Relative current change of the hydrogel sensor on the (e) applied compressive strain and (f) pressure. (g) Detection of different pressures ranging from 300 to 1000 kPa. (h) Detection of different bending angles.

Based on the excellent elasticity (Fig. 2a) and supercompressibility (Fig. 2b), the M-PVA hydrogel can be assembled as a compressible large-range sensor to detect the compressive strain and pressure stimuli. Upon compression, the distance of ionic migration shortened and the ionic channel widened, resulting in an obvious increasing conductivity of the hydrogel sensors. As illustrated in Fig. 5e, the hydrogel sensor exhibited sensitive electromechanical responses in a broad compressive strain range from 0 to 70%. When the compressive strain surpassed 70%, the current was too large to be detected by the oscilloscope. Fig. 5f demonstrates the dynamic current *versus* sustained pressure and the curve was divided into three sections according to the sensitivity. The sensitivity in the three sections was 6.23 Pa^{-1}, 0.72 Pa^{-1} and 0.26 Pa^{-1} within the pressure range of 0–0.29 MPa, 0.29–0.97 MPa and above 0.97 MPa, respectively. An illustration of the underlying reason for three different sensitivity regions is given in Fig. S6 (ESI†). The relative current change of the hydrogel sensor was approximately linearly related to the strain ranging from 0 to 70% (Fig. 5e). As for the compressive stress–strain curve, the pressure gradually augmented along with the increased strain. In the compressive strain range of 0–70%, the stress–strain curve was divided into three parts according to the curve slope, and the pressure ranges were 0–0.29 MPa, 0.29–0.97 MPa and 0.97–4.60 MPa, respectively (Fig. S6, ESI†). As a result, the relative current change *versus* pressure also was divided into three regions, which was consistent with the compressive stress–strain curve. The phenomenon of segmented sensitivity was similar to those in the previous studies.[23,25] Impressively, the pressure sensor was accurate under an ultrahigh pressure of as much as 4.60 MPa. As shown in Fig. 5g, the hydrogel pressure sensor responded ingeniously to different pressures (300–1000 kPa). The large-range detection range on compressive strain (0–70%) and pressure (0–4.60 MPa) is highly applicable in soft robots and heavy-duty machines.

Moreover, the detection capacity on bend deformation is a basic need for flexible sensors in practical applications. To study the bending sensitivity, the resistance of the hydrogel sensor was measured at different bending angles from 0° to 140°, as illustrated in the inset of Fig. 5h. The relative resistance change augmented monotonically with the increasing bending angles without noise fluctuation. When the bending angle increased to 140°, $\Delta R/R_0$ reached a high value of 350%.

The outstanding sensing performance on various deformations (elongation, compression and bend) and pressure will benefit the M-PVA hydrogel sensor to be utilized for full-range human-motion detection. To verify the feasibility, the M-PVA-1.6 hydrogel-based wearable sensor was fixed on various positions of the human body and the corresponding real-time electrical signals were recorded to monitor different human activities. As demonstrated in Fig. 6a, the hydrogel sensor was attached to the throat of a volunteer and subtle signals were perceived accurately when the volunteer spoke "gel". The hydrogel sensor can also recognize various joint movements. Every movement comprising bending and straightening of fingers can cause a change of relative resistance, and the relative resistance change pattern varied regularly (Fig. 6b). Similarly, the hydrogel sensor also produced a periodically sensitive response to the movement of the elbow and the knee (Fig. 6c and d). Additionally, the wearable hydrogel sensor can also be utilized in daily compression situations. As shown in Fig. 6e, repeated finger pressing produced stable and identical frequency signal patterns. Also, every gentle treading behavior of the volunteer was capable of producing a similar peak and valley in the current variation curve (Fig. 6f). The above results indicated that the M-PVA hydrogel-based sensor possessed excellent electrical stability and reliability for being a wearable device.

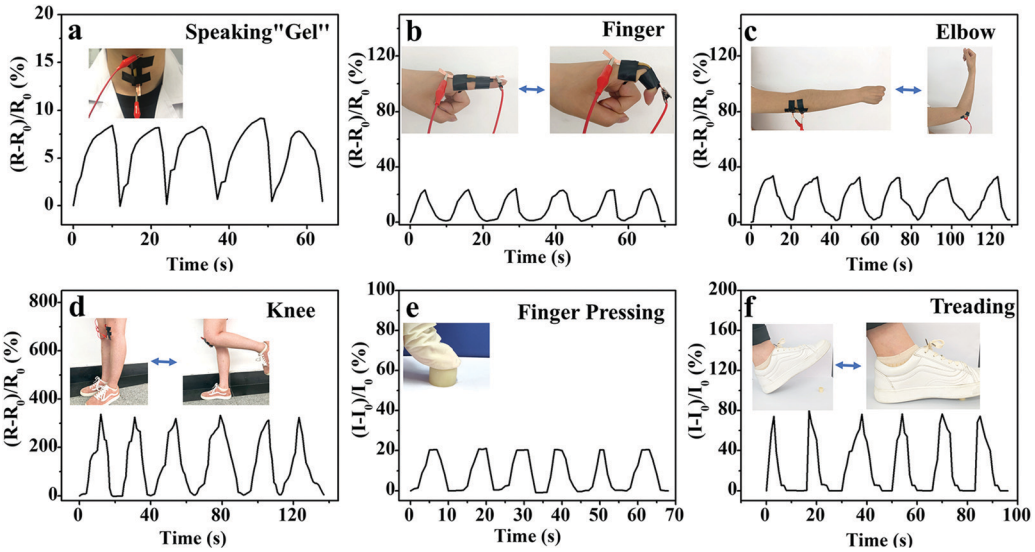

Fig. 6 Relative resistance variation of the M-PVA-1.6 hydrogel sensor that responded to (a) speaking behavior and various human joint movements: (b) finger, (c) elbow and (d) knee. The relative current changes of the hydrogel sensor upon (e) finger pressing and (f) gentle treading.

3.4 Anti-freezing performance of the M-PVA hydrogel

Generally, when the external environmental temperature decreases to below 0 °C, conductive hydrogels will inevitably enter a frozen state and therefore lose mechanical flexibility and conductivity, which greatly limits their practical applications. Recently, a class of low temperature tolerant hydrogels were proposed by incorporating ionic compounds such as calcium chloride ($CaCl_2$) to depress the freezing point of the aqueous phase.[29,43,44] The ions within the hydrogels can impair the aggregation of water molecules and weaken their internal hydrogen bonding, effectively hindering the formation of ice crystals in the hydrogels. Due to the incorporation of Fe^{3+} and SO_4^{2-} ions, the M-PVA hydrogel still maintained superior mechanical advantages and conductivity at subzero temperature. As shown in Fig. 7a, compared to the fragile frozen S-PVA hydrogel, the M-PVA hydrogel was very soft to be twisted easily after leaving in a refrigerator (−20 °C) for 3 days. Meanwhile, the M-PVA hydrogel was able to illuminate the light-emitting diode (LED) lamp even at −20 °C, whereas the S-PVA hydrogel cannot (Fig. 7b). The striking contrast between the S-PVA hydrogel and the M-PVA hydrogel confirmed that treatment with $Fe_2(SO_4)_3$ solution endowed the M-PVA hydrogel with excellent low temperature tolerance.

The mechanical properties of the M-PVA-1.6 gel at various temperatures were measured using an electromechanical universal testing machine equipped with an environmental chamber. Every gel specimen was held at the testing temperature for 30 min before measurement. Fig. 7c illustrates the tensile stress–strain curves of the M-PVA-1.6 gel within the temperature range from 25 to −50 °C. As the temperature decreased, ice crystals gradually emerged and

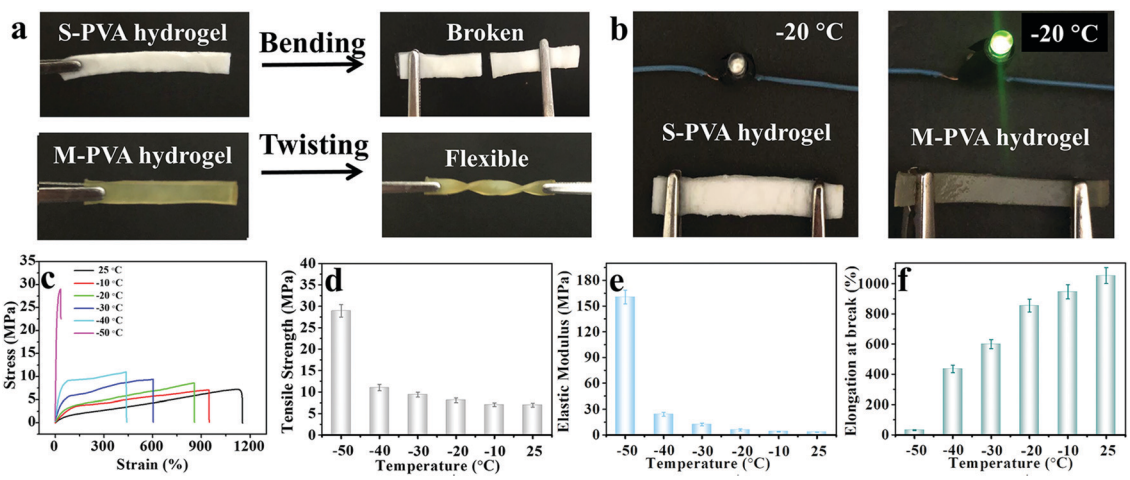

Fig. 7 (a) Frozen S-PVA gel and the soft M-PVA-1.6 hydrogel after leaving at −20 °C for 3 days. (b) Non-conductive S-PVA hydrogel and the conductive M-PVA-1.6 hydrogel in a closed circuit at −20 °C. (c) Tensile stress–strain curves of the M-PVA-1.6 gel within a broad temperature range from 25 to −50 °C. (d) Tensile strength, (e) elastic modulus and (f) elongation at break of the M-PVA-1.6 gel as a function of temperature.

the mobility of the polymer chains slowed down, resulting in a strong and stiff slurry gel. As shown in Fig. 7d–f, the tensile strength and elastic modulus of the M-PVA-1.6 gel increased sharply, whereas the fracture strain decreased quickly. Impressively, the M-PVA-1.6 gel still maintained remarkable stretchability at subzero temperature. Even at −40 °C, the M-PVA gel could be elongated to more than four times of the original length. As the temperature decreased to −50 °C, the M-PVA-1.6 gel almost converted into an aggregate of ice crystals and polymer chains with a negligible fracture strain of 30%. The outstanding mechanical deformability and conductivity of the M-PVA gel at low temperature was advantageous to explore its potential applications in harsh environments.

3.5 *In vivo* skin dressings

On account of the prominent anti-freezing performance in an extremely cold environment, the M-PVA hydrogel was considered to serve as a wearable dressing to protect the skin from frostbite in a harsh environment. In this work, an *in vivo* frostbite experiment was implemented on the rat skin as shown in Fig. 8A and B_1. The back skin of rats was divided into three regions: the (a) unprotected skin, (b) skin protected by the S-PVA hydrogel and (c) skin protected by the M-PVA hydrogel. Frostbite was induced by attaching extremely cold coins for 30 s, which were previously immersed in liquid nitrogen for 30 min. After the frostbite experiment, the M-PVA hydrogel still retained moisture, while the S-PVA hydrogel turned frozen (Fig. $8B_2$). Compared with obvious white frostbite eschar on the bare skin, the skin covered with the S-PVA hydrogel presented slight eschar, and the skin protected by the M-PVA hydrogel was similar to the normal skin (Fig. $8B_3$). Histological analysis further demonstrated the detailed condition of the epidermis and the dermis (Fig. 8C). As for the bare skin, part of

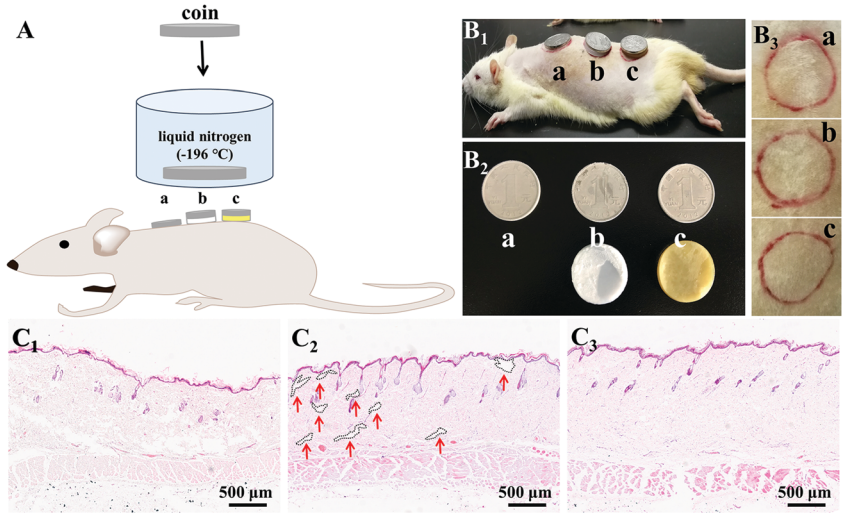

Fig. 8 (A) Schematics of the frostbite experiment on rat skins: the (a) unprotected skin, (b) S-PVA hydrogel-protected skin and (c) M-PVA hydrogel-protected skin. Photos of (B_1) *in vivo* frostbite experiment, (B_2) cold coins and hydrogels, and (B_3) skins after the frostbite experiment. (C) Histological microscopy images of the (C_1) bare skin, (C_2) S-PVA hydrogel-protected skin and (C_3) M-PVA hydrogel-protected skin.

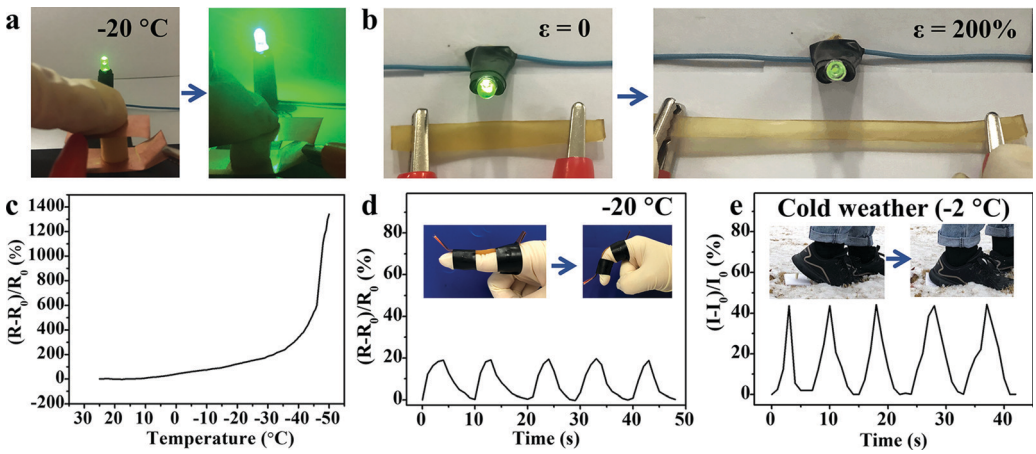

Fig. 9 Brightness variation of LED light in a circuit comprising the M-PVA-1.6 hydrogel upon (a) compression and (b) stretching at −20 °C. (c) Real-time relative resistance change of the anti-freezing M-PVA-1.6 hydrogel sensor during the cooling process. (d) Detection of finger bending at −20 °C. (e) Detection of treading behavior in cold weather.

the epidermis was destroyed and detached from the dermis, accompanied by a lot of voids and damaged hair follicles in the dermis. Conversely, the M-PVA hydrogel protected skin possessed an intact epidermal layer and dermis with intact collagen fibers, indicating normal skin tissue. The above results confirmed the great potential of M-PVA hydrogels as an anti-freezing dressing to protect the skin in an extreme low-temperature environment.

The unique attributes of high deformability and conductivity at low temperature enabled the M-PVA hydrogel to realize flexible sensing in a cold environment. As shown in Fig. 9a and Video S1 (ESI†), in spite of being placed at −20 °C for 24 h, the M-PVA-1.6 hydrogel was still conductive to power the LED bulb in a closed circuit and could respond to various external stimuli. When the M-PVA-1.6 hydrogel was pressed, the luminance of the LED bulb enhanced obviously. Conversely, the luminance of the LED bulb gradually dimmed as the hydrogel was stretched (Fig. 9b). The phenomena strongly indicated sensitive pressure and strain-dependent responsiveness at subzero temperature. In addition, the conductivity of the M-PVA-1.6 hydrogel showed temperature-dependent responsiveness (Fig. 9c). Along with the decreasing temperature, the limited mobility of the polymer chains and the generated ice crystal in the slurry gel impaired the ionic migration within the M-PVA-1.6 hydrogel, resulting in an increased resistance. Impressively, the hydrogel still can be utilized as an anti-freezing multi-model wearable sensor to detect human motion, such as finger movements at −20 °C (Fig. 9d) and treading behavior in cold weather (Fig. 9e). The regular and repeated curves strongly confirmed the feasibility and reliability of the M-PVA-1.6 hydrogel sensor at low temperature. As a consequence, the M-PVA hydrogel sensor can be utilized as freezing tolerant flexible wearable electronics for practical applications.

4. Conclusion

In summary, a high-mechanical, freeze tolerant and ionic conductive M-PVA hydrogel was constructed by importing chain entanglement and complexation between Fe^{3+} ions and hydroxyl groups into the microcrystalline network using immersion treatment in $Fe_2(SO_4)_3$ solution. Due to the synergistic effect of multiple physical crosslinking, the M-PVA hydrogel exhibited remarkable deformability in elongation (1120%) and compression (98%), superior strength, high toughness, impressively rapid self-recovery and anti-fatigue capacities. The incorporation of Fe^{3+} and SO_4^{2-} ions endowed the M-PVA hydrogel with good conductivity and eminent anti-freezing properties (low to −50 °C), which benefited the M-PVA hydrogel to act as a protective dressing in a harsh environment. The assembled multi-model hydrogel sensor was capable of detecting large range elongation (~900%), compression (~70%), bend and touched pressure (up to 4.60 MPa) with cycling stability and durability. Impressively, the wearable M-PVA hydrogel sensor can sensitively monitor various human activities, even in cold weather. Based on the feasible fabrication and fascinating features, the M-PVA hydrogel shows great potential for versatile applications in flexible electronics, motion recognition and intelligent robots within a broad temperature range.

Conflicts of interest

The authors declare no conflict of interest.

Acknowledgements

This work was supported by the National Natural Science Foundation of China (51803188), the China Postdoctoral Science Foundation (2018M642783 and 2019T120636), the Henan Postdoctoral Science Foundation (001801001) and the Key Scientific Research Projects of Colleges and Universities in Henan Province (19A430004) for financial support.

References

1 G. Shi, Z. Zhao, J. Pai, I. Lee, L. Zhang, C. Stevenson, K. Ishara, R. Zhang, H. Zhu and J. Ma, *Adv. Funct. Mater.*, 2016, **26**, 7614–7625.
2 H. Yuk, B. Lu and X. Zhao, *Chem. Soc. Rev.*, 2019, **48**, 1642–1667.
3 C. M. Boutry, A. Nguyen, Q. O. Lawal, A. Chortos, S. Rondeau-Gagne and Z. Bao, *Adv. Mater.*, 2015, **27**, 6954–6961.
4 J. Jia, J.-H. Pu, J.-H. Liu, X. Zhao, K. Ke, R.-Y. Bao, Z.-Y. Liu, M.-B. Yang and W. Yang, *Mater. Horiz.*, 2020, **7**, 2450–2459.
5 T. Q. Trung and N. E. Lee, *Adv. Mater.*, 2016, **28**, 4338–4372.
6 M. A. Darabi, A. Khosrozadeh, R. Mbeleck, Y. Liu, Q. Chang, J. Jiang, J. Cai, Q. Wang, G. Luo and M. Xing, *Adv. Mater.*, 2017, **29**, 1700533.
7 Y. Yang, Y. Wu, C. Li, X. Yang and W. Chen, *Adv. Intell. Syst.*, 2020, **2**, 1900077.
8 D. Chen and Q. Pei, *Chem. Rev.*, 2017, **117**, 11239–11268.
9 J.-W. Seo, H. Kim, K. Kim, S. Q. Choi and H. J. Lee, *Adv. Funct. Mater.*, 2018, **28**, 1800802.
10 Y. J. Hong, H. Jeong, K. W. Cho, N. Lu and D. H. Kim, *Adv. Funct. Mater.*, 2019, **29**, 1808247.
11 T. R. Hendricks, J. Lu, L. T. Drzal and I. Lee, *Adv. Mater.*, 2008, **20**, 2008–2012.
12 T. Sekitani, H. Nakajima, H. Maeda, T. Fukushima, T. Aida, K. Hata and T. Someya, *Nat. Mater.*, 2009, **8**, 494–499.
13 K. Sim, Z. Rao, F. Ershad and C. Yu, *Adv. Mater.*, 2020, **32**, 1902417.
14 X. Zhang, W. Liu, J. Cai, J. Huang and X. Qiu, *J. Mater. Chem. A*, 2019, **7**, 26917–26926.
15 J. J. Liang, L. Li, K. Tong, Z. Ren, W. Hu, X. F. Niu, Y. S. Chen and Q. B. Pei, *ACS Nano*, 2014, **8**, 1590–1600.
16 Y. Yu, Y. Luo, A. Guo, L. Yan, Y. Wu, K. Jiang, Q. Li, S. Fan and J. Wang, *Nanoscale*, 2017, **9**, 6716–6723.
17 T. Wang, Y. Zhang, Q. Liu, W. Cheng, X. Wang, L. Pan, B. Xu and H. Xu, *Adv. Funct. Mater.*, 2018, **28**, 170551.
18 V. R. Feig, H. Tran, M. Lee and Z. Bao, *Nat. Commun.*, 2018, **9**, 2740.

19 X. Sui, H. Guo, P. Chen, Y. Zhu, C. Wen, Y. Gao, J. Yang, X. Zhang and L. Zhang, *Adv. Funct. Mater.*, 2020, **30**, 190798.
20 Z. Liu, Y. Wang, Y. Ren, G. Jin, C. Zhang, W. Chen and F. Yan, *Mater. Horiz.*, 2020, **7**, 919–927.
21 Z. Wang, Y. Cong and J. Fu, *J. Mater. Chem. B*, 2020, **8**, 3437–3459.
22 L. Zhang, J. Zhao, J. Zhu, C. He and H. Wang, *Soft Matter*, 2012, **8**, 10439–10447.
23 H. Liu, X. Wang, Y. Cao, Y. Yang, Y. Yang, Y. Gao, Z. Ma, J. Wang, W. Wang and D. Wu, *ACS Appl. Mater. Interfaces*, 2020, **12**, 25334–25344.
24 Y. Chen, C. Jiao, X. Peng, T. Liu, Y. Shi, M. Liang and H. Wang, *J. Mater. Chem. B*, 2019, **7**, 3243–3249.
25 X. Zhang, N. Sheng, L. Wang, Y. Tan, C. Liu, Y. Xia, Z. Nie and K. Sui, *Mater. Horiz.*, 2019, **6**, 326–333.
26 G. Chen, J. Huang, J. Gu, S. Peng, X. Xiang, K. Chen, X. Yang, L. Guan, X. Jiang and L. Hou, *J. Mater. Chem. A*, 2020, **8**, 6776–6784.
27 B. Yang and W. Yuan, *ACS Appl. Mater. Interfaces*, 2019, **11**, 16765–16775.
28 H. Gao, Z. Zhao, Y. Cai, J. Zhou, W. Hua, L. Chen, L. Wang, J. Zhang, D. Han, M. Liu and L. Jiang, *Nat. Commun.*, 2017, **8**, 15911.
29 X. P. Morelle, W. R. Illeperuma, K. Tian, R. Bai, Z. Suo and J. J. Vlassak, *Adv. Mater.*, 2018, **30**, 1801541.
30 Q. Rong, W. Lei, L. Chen, Y. Yin, J. Zhou and M. Liu, *Angew. Chem., Int. Ed.*, 2017, **56**, 14159–14163.
31 S. Shi, X. Peng, T. Liu, Y.-N. Chen, C. He and H. Wang, *Polymer*, 2017, **111**, 168–176.
32 Z. Qin, D. Dong, M. Yao, Q. Yu, X. Sun, Q. Guo, H. Zhang, F. Yao and J. Li, *ACS Appl. Mater. Interfaces*, 2019, **11**, 21184–21193.
33 L. Han, K. Liu, M. Wang, K. Wang, L. Fang, H. Chen, J. Zhou and X. Lu, *Adv. Funct. Mater.*, 2018, **28**, 1704195.
34 X. Zhang, J. Huang, Z. Tang, B. Guo and L. Zhang, *Polymer*, 2020, **186**, 122059.
35 Y. Zhou, C. Wan, Y. Yang, H. Yang, S. Wang, Z. Dai, K. Ji, H. Jiang, X. Chen and Y. Long, *Adv. Funct. Mater.*, 2019, **29**, 1806220.
36 T. Liu, X. Peng, Y. Chen, J. Zhang, C. Jiao and H. Wang, *Polym. Chem.*, 2020, **11**, 4787–4797.
37 Y. Y. Yang, X. Wang, F. Yang, L. N. Wang and D. C. Wu, *Adv. Mater.*, 2018, **30**, 1707071.
38 S. Pan, M. Xia, H. Li, X. Jiang, P. He, Z. Sun and Y. Zhang, *J. Mater. Chem. C*, 2020, **8**, 2827–2837.
39 T. Yang, M. Wang, F. Jia, X. Ren and G. Gao, *J. Mater. Chem. C*, 2020, **8**, 2326–2335.
40 D. Rus and M. T. Tolley, *Nature*, 2015, **521**, 467–475.
41 Y. Yang, X. Wang, F. Yang, H. Shen and D. Wu, *Adv. Mater.*, 2016, **28**, 7178–7184.
42 Y. Yang, Y. Yang, Y. Cao, X. Wang, Y. Chen, H. Liu, Y. Gao, J. Wang, C. Liu, W. Wang, J.-K. Yu and D. Wu, *Chem. Eng. J.*, 2021, **403**, 126431.
43 X. F. Zhang, X. Ma, T. Hou, K. Guo, J. Yin, Z. Wang, L. Shu, M. He and J. Yao, *Angew. Chem., Int. Ed.*, 2019, **58**, 7366–7370.
44 Y. Yang, X. Wang and D. Wu, *Acta Chim. Sin.*, 2020, DOI: 10.6023/A20080370.

